Journal of Computational Applied Mechanics 2025, 56(3): 673-693

DOI: 10.22059/jcamech.2025.395958.1491

RESEARCH PAPER

Magneto-electro vibration analysis of a moderately thick double-curved sandwich panel with porous core and GPLRC using FSDT

Mohammad Ali Mohammadimehr [a], Abbas Loghman [a], Saeed Amir [a, *], Mehdi Mohammadimehr [a], Ehsan Arshid [b], Ömer Civalek [c]

[a] *Department of Solid Mechanics, Faculty of Mechanical Engineering, University of Kashan, Kashan, Iran, Postcode:87317-53153*

[b] *Faculty of Engineering, Mahallat Institute of Higher Education, Mahallat, Iran*

[c] *China Medical University Hospital, China Medical University, Taichung, Taiwan*

Abstract

In the present study, the magneto-electro vibration analysis of a moderately thick double-curved sandwich panel with porous core and graphene platelets reinforced composite (GPLRC) based on the nonlocal strain gradient theory (NSGT) is investigated. The displacement field of a moderately thick double-curved sandwich panel is considered as the first-order shear deformation theory (FSDT). The equations of motion are derived using Hamilton's principle and these equations are solved by Navier's method. The effect of various parameters, including magnetic and electric fields, aspect ratio, core-to-face thickness ratio, volume fraction of GPLs, different porosity distributions, various GPLs distributions, and curvature radius on the dimensionless natural frequencies of a moderately thick doubly-curved sandwich panel is examined. In this research, the sandwich structures become consist of two thin face sheets with high strength and a thick, soft, and flexible core with low density, because the scientists follow to enhance the strength to weight in the sandwich structures that these structures are used in various industries. In this article, the doubly-curved sandwich panel includes cylindrical, spherical, and elliptical shapes. The main finding of this research is that the dimensionless natural frequency reaches its maximum value at $h_c / h_f = 6$.

Keywords: Magneto-electro vibration; Moderately thick double-curved sandwich panel; Porous core; GPLs; Nonlocal strain gradient theory and First-order shear deformation theory.

1. Introduction

In recent decades, researchers have focused on sandwich structures to improve their strength-to-weight ratio. This study examines sandwich structures with a soft core, reinforced by graphene platelets (GPLs) in the matrix. Due to their high strength-to-weight ratio, these structures are widely used in industries such as aerospace, aviation,

* Corresponding author..*E-mail address:* Saeed Amir, samir@kashanu.ac.ir, saeedamir2000@gmail.com

automotive, and the body of ship. Some researchers [1-5] studied spherical vibrations and investigated the effects of boundary conditions (mechanical), geometry (thickness), various polar angles, different materials, material length scale parameter, temperature gradient, and specific heat capacity in constant volume on the natural frequency. The cylindrical vibrations are analyzed by some researchers [6-10] and investigated the effect of external loads amplitude, isolators, damping, the taper wedge compared to uniform wedge, external excitation frequency, random excitation strength, harmonic excitation, geometric and material properties, the number of circumferential and axial waves, and the multi-layer method on the natural frequency. Some scientists [11-15] analyzed vibrations under magnetic and electric fields and studied the effects of parameters such as the intensity of the magnetic and electric fields, multi-physical loads, the type and geometric properties of the panel, different materials, and the control coefficients of the electrical and magnetic fields, electric and magnetic potentials on the vibration control of sandwich shells. One of their results is that with increasing the magnetic power, the area of the convective cells reduces. The vibrations of porous panels [16-20] are investigated and showed the effect of aspect ratio and geometry, porosity parameter, complete and partial porosity, the shape and distribution pattern of the porosity area on the natural frequency. They found that the natural frequency decreases by 15 to 18 percentage, when the porosity increases to 70%. Some researchers [21-25] analyzed vibrations based on nonlocal strain gradient theory and investigated the effects of material length scale parameter, size-dependent effects, and Eringen's nonlocal parameter on the natural frequency. They demonstrated that inverse phenomena are created by the effect of the nonlocal strain gradient. Some scientists [26-30] investigated the vibrations of thick panels that the effect of the fluid on the nonlinear behavior of the system decreases with increasing shell thickness, and the behavior of the shell becomes more dominant in the system. Another of their result is that for thicker plates, the frequency and amplitude of vibrations increases and decreases, respectively. Also, they investigated the effect of crack position, crack length on the vibrations of thick plates and the effects of core thickness, boundary conditions, temperature-dependent material properties and temperature gradients in the thickness direction on the dynamic characteristics. The vibrations of shallow shells [31-36] and the effects of porosity coefficient, boundary conditions, geometric parameters, elastic foundation, orthotropy, nonlinearity, shear stresses, types of carbon nanotube distribution, number of reinforcements, and scale dependence on the dynamic response and natural frequencies of the system are investigated. The vibration of shells and panels reinforced with graphene platelets (GPLs) and carbon nanotubes (CNTs) by some researchers [13, 37-40] were studied, and they investigated the effects of factors such as the reinforcement distribution pattern of GPLs and CNTs, weight fraction, volume fraction index of GPLs and CNTs, number of layers, elastic foundation parameters, external electric voltage and magnetic potential, geometrical parameters such as layers thickness and physical parameters such as temperature changes and Winkler foundation on the natural frequency of the system. One of their results was that the stiffness, with the weight fraction without a change in mass increases.

The novelty of this research lies in the simultaneous investigation of a moderately thick double-curved sandwich shells with a porous core and graphene platelets under magnetic and electric fields, based on first-order shear deformation theory. The equations of motion for the sandwich panel have derived using Hamilton's principle and the extended mixture rule. The effects of various parameters, such as the geometric dimensions of the doubly-curved panel, different porosity distributions, porosity coefficient, various GPL distributions, volume fraction of GPL, and magnetic and electric fields on the dimensionless natural frequency have evaluated.

1. Geometry and material properties of a sandwich panel

Fig. 1 shows a moderately thick double-curved sandwich panel with porous core and GPL reinforced composite (GPLRC) in face sheets layers. It is shown that the thickness of the porous core, top and bottom face sheet are h_c, h_t, and h_b , respectively. The total thickness denotes h,. L_x , L_y are the length of double-curved sandwich panel. x , y , z are the curve linear coordinate axes. Also, a and b show the arc length of the sandwich panel. Moreover, ϕ and R_x , R_y are panel angle, and the curvature radii of the sandwich panel.

The relationships between different porous core structures; including uniform porosity, symmetric (type 1), and asymmetric porosity (type 2) are expressed as follows [41]:

$$
\begin{aligned}
&E_c(z) = E_1^c(1-e_0\lambda) \\
&\rho_c(z) = \rho_1^c(1-e_m\lambda) \\
&\lambda = \cos(\pi z/h_c) && \text{Type 1} \\
&\lambda = \cos(\pi z/h_c + \pi/4) && \text{Type 2} \\
&\lambda = \frac{1}{e_0} - \frac{1}{e_0}\left(\frac{2}{\pi}\sqrt{1-e_0} - \frac{2}{\pi} + 1\right)^2 && \text{Type 3}
\end{aligned}
\tag{1}
$$

where ρ_1^c and E_1^c denote values of mass density and Young's modulus of the pure metal core.

The various distribution types of GPLs for the lower and upper layers are defined as follows [42]: In this section, three different types of GPL distribution are considered: symmetric distribution (GPL-S), and asymmetric distribution (GPL-A), uniform distribution (GPL-U). The volume fraction patterns are defined below:

$$
V_{GPL} = \begin{Bmatrix} V_{GPL}^{*} & \rightarrow GPL-U \\ V_{GPL}^{*}\left[1-\cos\left(\dfrac{\pi(4z+h)}{4h}\right)\right] & \rightarrow GPL-A \\ V_{GPL}^{*}\left[1-\cos\left(\dfrac{\pi z}{h}\right)\right] & \rightarrow GPL-S \end{Bmatrix}
\tag{2}
$$

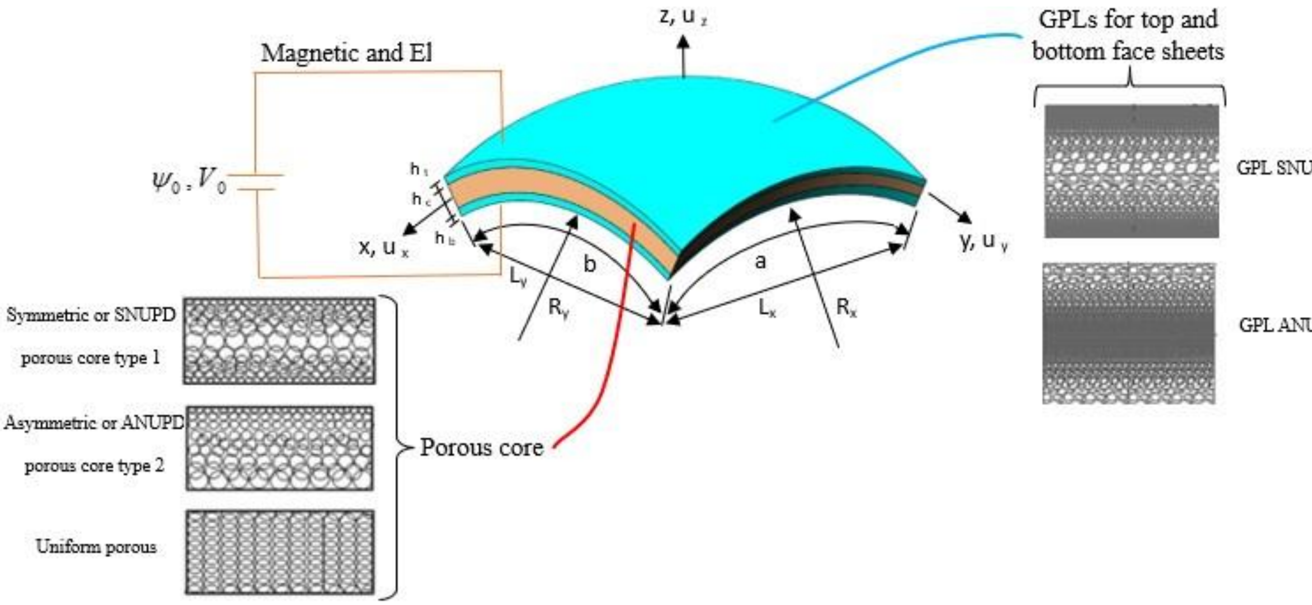

Fig. 1: A schematic view of a moderately thick double-curved sandwich panel with porous core and graphene platelet face sheets

Also, the material properties for the extended rule of mixture are written as follows [42]:

$$E_{11}=\eta_1 V_{GPL} E_{11}^{GPL}+V_m E^m$$
$$\frac{\eta_2}{E_{22}}=\frac{V_{GPL}}{E_{22}^{GPL}}+\frac{V_m}{E^m}$$
$$\frac{\eta_3}{G_{12}}=\frac{V_{GPL}}{G_{12}^{GPL}}+\frac{V_m}{G^m} \tag{3}$$
$$V_m+V_{GPL}^{*}=1$$

where $E_{11}^{GPL}=5.6466\,TPa$, $E_{22}^{GPL}=7.08\,TPa$ and $E^m=2.5\,GPa$ are the elastic modulus for GPL and the matrix, respectively, and also, $G_{12}^{GPL}=1.9445\,TPa$ and $G^m=E^m/2(1+\upsilon^m)$ where $\upsilon^m=0.3$ are the shear modulus for GPL and matrix Poisson's ratio of a matrix, respectively. In addition, η_1, η_2, η_3 represent the efficiency parameters of GPL, incorporating the size-dependent material properties [42].

The mechanical properties of the porous core and GPL face sheets for a moderately thick double-curved thick sandwich panel are considered in Table 1.

Table 1: The mechanical properties of GPL face sheets [42] **and porous core** [43] **for sandwich panel**

GPL face sheets	Porous core
$E_{GPL}=1.01\ TPa$ $\rho_{GPL}=1062.5\ kg/m^3$ $\upsilon_{GPL}=0.186$	$\rho_c=97\ kg/m^3$ $E_1=E_2=E_3=6.89\ MPa$ $G_{12}=G_{13}=G_{23}=3.45\ MPa$ $\upsilon_{12}=\upsilon_{13}=\upsilon_{23}=0$

which V_{GPL}^{*} is obtained [42].

2. The governing equations of motion for a moderately thick double-curved sandwich panel

The displacement fields for a moderately thick double-curved sandwich panel are assumed as Eq. (4) [21, 44]

$$\begin{Bmatrix} u_x \\ u_y \\ u_z \end{Bmatrix}=\begin{cases} u(x,y,t)+z\,\phi_x(x,y,t) \\ v(x,y,t)+z\,\phi_y(x,y,t) \\ w(x,y,z,t) \end{cases} \tag{4}$$

where u_x, u_y and u_z are the components of displacements at a distance z from the middle plane. u and v are the membrane displacements in middle plane, and w is the transverse displacement. Also, ϕ_x and ϕ_y show the slope of a moderately thick double-curved sandwich panel.

The strain-displacement relations for the moderately thick double-curved sandwich panel are written as follows:

$$\begin{aligned}\varepsilon_{xx}&=\frac{1}{1+z/R_x}(u_{1,x}+\frac{u_3}{R_x}) \\ &=\frac{1}{1+z/R_x}\left[(1+z/R_x)u_{,x}+z\phi_{x,x}-z^3c_1(1+\frac{h^2}{4R_x^2})(\phi_x+w_{,x})_{,x}+\frac{w}{R_x}\right]\end{aligned} \tag{5a}$$

(5b)

$$\varepsilon_{yy} = \frac{1}{1+z/R_y}(u_{2,\mathrm{y}} + \frac{u_3}{R_y}) \tag{5c}$$

$$= \frac{1}{1+z/R_y}\left[(1+z/R_y)v_{,\mathrm{y}} + z\phi_{\mathrm{y,y}} - z^3 c_2 (1+\frac{h^2}{4R_y^2})(\phi_y + w_{,\mathrm{y}})_{,\mathrm{y}} + \frac{w}{R_y}\right] \tag{6a}$$

$$\varepsilon_{zz} = 0$$

$$\gamma_{xz} = u_{1,z} + \frac{1}{1+z/R_x}(w_{,x} - \frac{u_1}{R_y})$$

$$= \frac{u}{R_x} + \phi_x - 3z^2 c_1 (1+\frac{h^2}{4R_x^2})(\phi_x + w_{,x})$$

$$+ \frac{1}{1+z/R_x}\left[w_{,x} - (1+z/R_x)\frac{u}{R_x} - \frac{z\phi_x}{R_x} + z^3 \frac{c_1}{R_x}(1+\frac{h^2}{4R_x^2})(\phi_x + w_{,x})\right] \tag{6b}$$

$$\gamma_{yz} = u_{2,z} + \frac{1}{1+z/R_y}(w_{,\mathrm{y}} - \frac{u_2}{R_y})$$

$$= \frac{v}{R_y} + \phi_y - 3z^2 c_2 (1+\frac{h^2}{4R_y^2})(\phi_y + w_{,\mathrm{y}}) \tag{6c}$$

$$+ \frac{1}{1+z/R_y}\left[w_{,\mathrm{y}} - (1+z/R_y)\frac{v}{R_y} - \frac{z\phi_y}{R_y} + z^3 \frac{c_2}{R_y}(1+\frac{h^2}{4R_y^2})(\phi_y + w_{,\mathrm{y}})\right]$$

$$\gamma_{xy} = \frac{1}{1+z/R_x}(u_{2,x}) + \frac{1}{1+z/R_y}(u_{1,\mathrm{y}})$$

$$= \frac{1}{1+z/R_x}\left[(1+z/R_y)v_{,x} + z\phi_{y,\mathrm{x}} - z^3 c_2 (1+\frac{h^2}{4R_y^2})(\phi_y + w_{,\mathrm{y}})_{,x}\right]$$

$$= \frac{1}{1+z/R_y}\left[(1+z/R_x)u_{,y} + z\phi_{x,y} - z^3 c_1 (1+\frac{h^2}{4R_x^2})(\phi_x + w_{,x})_{,y}\right]$$

where R_x, R_y are the radius of the panel from the center to the middle of the core for double-curved panel including spherical $R_y = R_x$, ellipsoidal $R_y = 1.5\,R_x$, cylindrical $R_x = R$, $R_y = \infty$. ε_x, ε_y, and ε_z are the components of normal strain and γ_{xy}, γ_{xz} and γ_{yz} are the components of shear strain.

The constitutive equations along the off-axis coordinate based on nonlocal strain gradient theory (NSGT) are obtained as follows [45]:

$$\left(1-(e_0 a)^2\nabla^2\right)\sigma_{ij} = (1-l_m^2\nabla^2)C_{ijkl}\varepsilon_{kl} - e_{kij}E_k - q_{kij}H_k \quad i,j = x,y,z;\ k,l = x,y,z \tag{7}$$

$$D_i = e_{ikl}\,\varepsilon_{kl} + s_{ik}E_k + d_{ik}H_k \tag{8}$$

$$B_i = q_{ikl}\,\varepsilon_{kl} + d_{ik}E_k + \mu_{ik}H_k \tag{9}$$

where l_m and e_0a denote the strain gradient and nonlocal parameters based on nonlocal strain gradient theory. ∇^2 is the Laplacian operator. C_{ijkl} denotes the fourth-order stiffness tensor along the off-axis coordinates. ε_{kl} and σ_{ij} are the components of strain and stress along the off-axis coordinates. Also e_{ikl}, q_{ikl}, s_{ik}, d_{ik} and μ_{ik} are piezoelectric, magnetic, dielectric permeability, electromagnetic coupling, magnetic permeability.

The kinematic energy for a moderately thick double-curved sandwich panel based on FSDT is written as follows [21, 44]:

$$\int_{t_1}^{t_2} (\delta T - (\delta U + \delta W_{ext}))dt = 0 \tag{11}$$

where δT, δU and δW_{ext} are the variations of the kinetic energy, strain energy, and potential energy due to the work of the external force.

The variations of the kinematic energy and the strain energy for the moderately thick double-curved sandwich panel based on FSDT are considered as follows [44-46]:

$$\begin{aligned}\delta T &= \delta \int_V \left(\frac{1}{2}\rho \dot{u}_1{}^2 + \frac{1}{2}\rho \dot{u}_2{}^2 + \frac{1}{2}\rho \dot{u}_3{}^2 \right) R_x R_y (1+z/R_x)(1+z/R_y)\, dx\, dy\, dz \\ &= \int_V (\rho \dot{u}_1 \delta \dot{u}_1 + \rho \dot{u}_2 \delta \dot{u}_2 + \rho \dot{u}_3 \delta \dot{u}_3) R_x R_y (1+z/R_x)(1+z/R_y)\, dx\, dy\, dz\end{aligned} \tag{12}$$

where ρ is mass density and $\dot{u}_i\,(i = x, y, z)$ is velocity along the coordinate axes of a moderately thick double-curved sandwich panel.

$$\delta U = \int_V \begin{pmatrix} \sigma_x \delta\varepsilon_x + \sigma_y \delta\varepsilon_y + \sigma_z \delta\varepsilon_z + \tau_{xy} \delta\gamma_{xy} \\ +\tau_{yz} \delta\gamma_{yz} + \tau_{xz} \delta\gamma_{xz} - D_x \delta E_x - D_y \delta E_y \\ -D_z \delta E_z - B_x \delta H_x - B_y \delta H_y - B_z \delta H_z \end{pmatrix} R_x R_y (1+z/R_x)(1+z/R_y)\, dx\, dy\, dz \tag{13}$$

$$E = -\nabla \phi \quad , \quad H = -\nabla \Psi \tag{14}$$

The variation of the external work based on multi-physics including magneto-electro-mechanical loadings is defined as follows [47]:

$$\delta W_{ext} = \int \left[\left(N_{p_x} + N_{E_x} + N_{M_x} \right) \frac{\partial^2 w}{\partial x^2} + \left(N_{p_y} + N_{E_y} + N_{M_y} \right) \frac{\partial^2 w}{\partial y^2} \right] \delta w\, dA \tag{15}$$

in which N_{px} and N_{py} indicate pressure preload in the x and y directions. Moreover, electrical and magnetic preloads are indicated as N_E and N_M. The relations of the vectors and tensors are specified as [48]:

The preload relations for a sandwich panel can be written as [49]:

$$\begin{aligned} &N_{p_x} = N_{p_y} = P_0 \;,\; N_{M_x} = N_{M_y} = -2 f_{31} \psi_0 \;,\; f_{31} = 290.2 \;\; N/A.m \;,\; \psi_0 = 12.5\, A \\ &,\; N_{E_x} = N_{E_y} = -2 e_{13} V_0 \;,\; e_{13} = \text{-}4.1\; C/m^2 \;,\; V_0 = 1.5\, V \end{aligned} \tag{16}$$

in which P_0 is biaxial force, and inertial electric voltage and magnetic potential are presented by V_0 and Ψ_0. All components of the above equations are calculated.

$$\Psi = (x,y,z,t) = \frac{2\bar{z}}{h_p}\psi_0 - \psi(x,y,t)\cos\left(\frac{\pi \bar{z}}{h_p}\right) \;,\; \Phi = (x,y,z,t) = \frac{2\bar{z}}{h_p}\phi_0 - \phi(x,y,t)\cos\left(\frac{\pi \bar{z}}{h_p}\right) \tag{17}$$

The resultant forces and moments of a moderately thick double-curved sandwich panel are expressed as follows:

$$\begin{Bmatrix} N_x^i \\ S_{xz}^i \\ S_{xy}^i \end{Bmatrix} = \int \begin{Bmatrix} \sigma_x \\ \tau_{xz} \\ \tau_{xy} \end{Bmatrix} (1 + z/R_y)\, z^i dz \qquad i = 0,1,3$$

$$\begin{Bmatrix} N_y^i \\ S_{yz}^i \\ P_{xy}^i \end{Bmatrix} = \int \begin{Bmatrix} \sigma_y \\ \tau_{yz} \\ \tau_{xy} \end{Bmatrix} (1 + z/R_x)\, z^i dz \qquad i = 0,1,3 \tag{18}$$

$$\begin{Bmatrix} M_{yz}^i \\ M_{xz}^i \end{Bmatrix} = \int \begin{Bmatrix} \tau_{yz} \\ \tau_{xz} \end{Bmatrix} (1 + z/R_x)(1 + z/R_y) z \qquad i = 0,2$$

where the above variables show the resultant axial/shear forces and bending/torsion moments of a moderately thick double-curved sandwich panel.

The coefficients of the mass moment of inertia for the sandwich panel are calculated as follows:

$$I^{*i} = \int \rho (1 + z/R_x)(1 + z/R_y) z^i dz \qquad i = 0,1,2,3,4,6$$

where I^{*i} are the mass moments of inertia for a moderately thick double-curved sandwich panel.

The stiffness coefficients of a moderately thick double-curved sandwich panel with a porous core and nanocomposite tops reinforced with GPLs are described in Appendix A. The coefficients of the mass matrix for the sandwich panel are shown in Appendix B.

The equations of motion for a moderately thick double-curved sandwich panel with a porous core and nano-composite face sheets reinforced by GPLs are obtained as follows:

$$\delta u \ : \ (1 - l_m^2 \nabla^2)\{ -\frac{\partial}{\partial x} N_x^0 - \frac{1}{R_x} S_{xz}^0 - \frac{\partial}{\partial y} P_{xy}^0 \} + (1 - (e_0 a)^2 \nabla^2)\{ I^{*0} \frac{\partial^2 u}{\partial t^2} + I^{*1} \frac{\partial^2 \phi_x}{\partial t^2} \} = 0$$

$$\delta v \ : \ (1 - l_m^2 \nabla^2)\{ -\frac{\partial}{\partial y} N_y^0 - \frac{1}{R_y} S_{yz}^0 - \frac{\partial}{\partial x} S_{xy}^0 \} + (1 - (e_0 a)^2 \nabla^2)\{ I^{*0} \frac{\partial^2 v}{\partial t^2} + I^{*1} \frac{\partial^2 \phi_y}{\partial t^2} \} = 0$$

$$\delta w \ : \ (1 - l_m^2 \nabla^2)\{ \frac{N_x^0}{R_x} + \frac{N_y^0}{R_y} - \frac{\partial}{\partial y} S_{yz}^0 - \frac{\partial}{\partial x} S_{xz}^0 \} + (1 - (e_0 a)^2 \nabla^2)\{ I^{*0} \frac{\partial^2 w}{\partial t^2} \} = 0$$

$$\delta \phi_x \ : \ (1 - l_m^2 \nabla^2)\{ -\frac{\partial}{\partial x} N_x^1 + M_{xz}^0 - \frac{1}{R_x} S_{xz}^1 - \frac{\partial}{\partial y} P_{xy}^1 \} + (1 - (e_0 a)^2 \nabla^2)\{ I^{*1} \frac{\partial^2 u}{\partial t^2} + I^{*2} \frac{\partial^2 \phi_x}{\partial t^2} \} = 0 \tag{20-1}$$

$$\delta \phi_y \ : \ (1 - l_m^2 \nabla^2)\{ -\frac{\partial}{\partial y} N_y^1 + M_{yz}^0 - \frac{1}{R_y} S_{yz}^1 - \frac{\partial}{\partial x} S_{xy}^1 \} + (1 - (e_0 a)^2 \nabla^2)\{ I^{*1} \frac{\partial^2 v}{\partial t^2} + I^{*2} \frac{\partial^2 \phi_y}{\partial t^2} \} = 0$$

$$\delta \phi \ : \ \frac{\partial}{\partial x} D_x + \frac{\partial}{\partial y} D_y + \bar{D}_z = 0$$

$$\delta \psi \ : \ \frac{\partial}{\partial x} B_x + \frac{\partial}{\partial y} B_y + \bar{B}_z = 0 \tag{20-2}$$

$$\bar{D}_z = \int \frac{\partial}{\partial z} D_z \, dz \quad , \quad \bar{B}_z = \int \frac{\partial}{\partial z} B_z \, dz \tag{21}$$

Assuming the following equations and placing the resulting forces and moments in the equations of motion, the governing equations of motion for a double-curved thick sandwich panel with porous core and nanocomposite face sheets reinforced by GPL based on first-order shear deformation double-curved theory (FSDT) and NSGT are considered in the Appendix C.

The displacement functions based on Navier's solution are defined in Eq. (22). where ω_{mn} is the natural frequency for a moderately thick double-curved sandwich panel. Also, the coefficients of α_m and β_n are defined in Eq. (23). where m and n are the wave numbers in *x* and *y* directions, respectively. Also, L_x and L_y denote the length of a moderately thick double-curved sandwich panel in *x* and *y* directions, respectively.

$$\begin{aligned}
u(x,y,\mathrm{t}) &= \sum_{m=1}^{\infty}\sum_{n=1}^{\infty} u_{mn} \cos(\alpha_m x)\sin(\beta_n y) e^{i\omega_{mn}t}, \\
v(x,y,\mathrm{t}) &= \sum_{m=1}^{\infty}\sum_{n=1}^{\infty} v_{mn} \sin(\alpha_m x)\cos(\beta_n y) e^{i\omega_{mn}t} \\
w(x,y,\mathrm{t}) &= \sum_{m=1}^{\infty}\sum_{n=1}^{\infty} w_{mn} \sin(\alpha_m x)\sin(\beta_n y) e^{i\omega_{mn}t}, \\
\phi_x(x,y,\mathrm{t}) &= \sum_{m=1}^{\infty}\sum_{n=1}^{\infty} \phi_{x\,mn} \cos(\alpha_m x)\sin(\beta_n y) e^{i\omega_{mn}t}, \\
\phi_y(x,y,\mathrm{t}) &= \sum_{m=1}^{\infty}\sum_{n=1}^{\infty} \phi_{y\,mn} \sin(\alpha_m x)\cos(\beta_n y) e^{i\omega_{mn}t}, \\
\phi(x,y,\mathrm{t}) &= \sum_{m=1}^{\infty}\sum_{n=1}^{\infty} \phi_{mn} \sin(\alpha_m x)\sin(\beta_n y) e^{i\omega_{mn}t}, \\
\psi(x,y,\mathrm{t}) &= \sum_{m=1}^{\infty}\sum_{n=1}^{\infty} \psi_{mn} \sin(\alpha_m x)\sin(\beta_n y) e^{i\omega_{mn}t},
\end{aligned} \tag{22}$$

$$\alpha_m = \frac{m\pi}{L_x} \quad , \quad \beta_n = \frac{n\pi}{L_y} \tag{23}$$

By substituting Eq. (23) into Eqs. (D-1) and (D-2), the stiffness and mass matrices for a moderately thick double-curved sandwich panel are obtained as follows:

$$\left([K]_{7x7} - \omega_{mn}^2 [M]_{7x7}\right)\{u\}_{7x1} = \underset{\sim}{0} \tag{24}$$

$$K=(1-l_m^2)(\alpha_m^2+\beta_n^2)\begin{bmatrix} K_{11} & K_{12} & K_{13} & K_{14} & K_{15} & K_{16} & K_{17} \\ K_{21} & K_{22} & K_{23} & K_{24} & K_{25} & K_{26} & K_{27} \\ K_{31} & K_{32} & K_{33} & K_{34} & K_{35} & K_{36} & K_{37} \\ K_{41} & K_{42} & K_{43} & K_{44} & K_{45} & K_{46} & K_{47} \\ K_{51} & K_{52} & K_{53} & K_{54} & K_{55} & K_{56} & K_{57} \\ K_{61} & K_{62} & K_{63} & K_{64} & K_{65} & K_{66} & K_{67} \\ K_{71} & K_{72} & K_{73} & K_{74} & K_{75} & K_{76} & K_{77} \end{bmatrix},$$

$$M=[1-(e_0\,\mathrm{a})^2](\alpha_m^2+\beta_n^2)\begin{bmatrix} M_{11} & M_{12} & M_{13} & M_{14} & M_{15} & M_{16} & M_{17} \\ M_{21} & M_{22} & M_{23} & M_{24} & M_{25} & M_{26} & M_{27} \\ M_{31} & M_{32} & M_{33} & M_{34} & M_{35} & M_{36} & M_{37} \\ M_{41} & M_{42} & M_{43} & M_{44} & M_{45} & M_{46} & M_{47} \\ M_{51} & M_{52} & M_{53} & M_{54} & M_{55} & M_{56} & M_{57} \\ M_{61} & M_{62} & M_{63} & M_{64} & M_{65} & M_{66} & M_{67} \\ M_{71} & M_{72} & M_{73} & M_{74} & M_{75} & M_{76} & M_{77} \end{bmatrix}, \quad \underset{\sim}{u}=\begin{Bmatrix} u_{mn} \\ v_{mn} \\ w_{mn} \\ \phi_{x\,mn} \\ \phi_{y\,mn} \\ \phi_{mn} \\ \psi_{mn} \end{Bmatrix} \tag{25}$$

So, the stiffness and mass matrices are described in Appendix D.

The vibration analysis of a moderately thick double-curved sandwich panel with a porous core and nanocomposite face sheets reinforced by GPLs based on NSGT and FSDT is investigated. The effect of different parameters such as the material length scale parameter, the non-local Eringen's parameter, the different angles of the porous core, the volume fraction of GPLs, and its various distributions for different double-curved structures, including spherical, ellipsoidal, cylindrical, and plate, on the dimensionless natural frequency are studied.

In this study, ϖ is the dimensionless natural frequency that is defined as follows:

$$\varpi=\omega_{mn}h\sqrt{\frac{\rho_c}{E_c}} \tag{26}$$

in which h is the total thickness of a sandwich panel and ρ_c , E_c shows the density and elastic modulus of the porous core, respectively.

The geometry of a double-curved thick sandwich panel is shown in Table 2.

Table 2: The geometry of a double-curved thick sandwich panel

$L_x=L_y=200\ \mu m$
R_x *and* R_y *are* var*ious*
$h=0.25L_x$
$h_c/h_f=2$ *to* 18

The results of this research have been validated by the other literature by Sayyad and Ghugal [50]. This validation is shown in Table 3. It is seen that there is a good agreement between them.

Fig. 2 shows that the dimensionless natural frequency for a cylindrical panel with a porous core and graphene platelets face sheets is higher than that of a spherical panel. Additionally, the dimensionless frequency for the spherical panel is directly related to the curvature radius, meaning that as the curvature radius of the sphere increases, the dimensionless frequency increases. For the cylindrical panel, however, there is an inverse relationship as the curvature radius of the cylinder increases, the dimensionless frequency decreases. Moreover, the smaller the ratio of the porous core thickness to the graphene platelet thickness, the higher the dimensionless natural frequency.

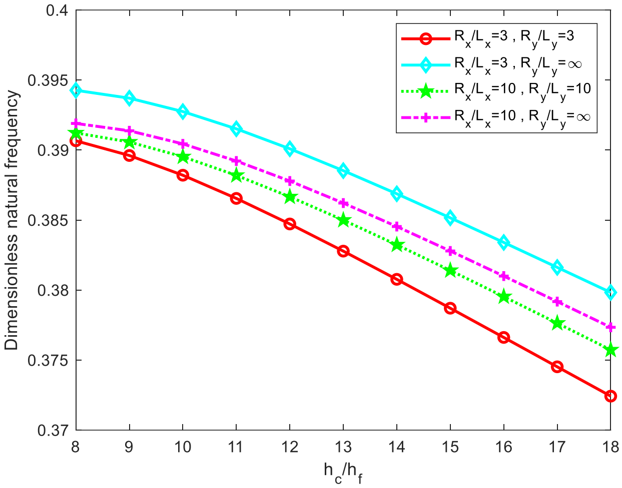

Fig. 2: Dimensionless natural frequency of spherical and cylindrical sandwich panel

Fig. 3 shows the effect of different distribution of graphene platelets on dimensionless natural frequency of a moderately thick sandwich panel. It is shown that the symmetric graphene platelets face sheet has the highest dimensionless natural frequency, followed by the asymmetric graphene platelet and then the uniform graphene platelet. Additionally, a ratio of $h_c/h_f = 6$ has the highest dimensionless natural frequency.

Table 3: The dimensionless natural frequency for the present work and th3e obtained results by Sayyad and Ghugal [57] ($\omega^{**} = \omega_{mn} h \sqrt{\frac{\rho_c}{E_c}}$) based on FG of double-curved

($a = b, a/h = 5, p = 2, E_c = 380\,GPa,\ \rho_c = 3800\,kg/m^3,\ E_m = 70\,GPa,\ \rho_m = 2707\,kg/m^3,\ \mu = 0.3$

Type of Shells	R_x/a	R_y/b	PSDT	TSDT	HSDT	ESDT	FSDT	CST	Present
Cylindrical Shells	5	∞	0.14759	0.14759	0.14760	0.14763	0.14996	0.15990	0.14968
	10	∞	0.14739	0.14739	0.14739	0.14742	0.14978	0.15980	0.14948
	20	∞	0.14738	0.14741	0.14739	0.14742	0.14978	0.15984	0.14948
	50	∞	0.14741	0.14742	0.14741	0.14744	0.14981	0.15988	0.14951
	100	∞	0.14743	0.14936	0.14743	0.14746	0.14983	0.15990	0.14953
Spherical Shells	5	5	0.14936	0.14775	0.14936	0.14939	0.15168	0.16136	0.15146
	10	10	0.14775	0.14743	0.14775	0.14778	0.15012	0.16006	0.14984
	20	20	0.14743	0.14739	0.14743	0.14746	0.14982	0.15984	0.14952
	50	50	0.14740	0.14741	0.14740	0.14743	0.14980	0.15986	0.14950
	100	100	0.14741	0.14682	0.14741	0.14744	0.14982	0.15988	0.14951
Elliptical paraboloid Shellls	5	7.5	0.14867	0.14866	0.14867	0.14870	0.15100	0.16079	0.15076
	10	15	0.14760	0.14760	0.14760	0.14763	0.14998	0.15995	0.14969
	20	30	0.14741	0.14740	0.14741	0.14744	0.14980	0.15984	0.14950
	50	75	0.14740	0.14740	0.14740	0.14743	0.14980	0.15986	0.14950
	100	150	0.147	0.147	0.147	0.147	0.149	0.159	0.14952

	42	41	42	45	82	89

Fig. 4 shows the effect of various porosity distributions including uniform distribution on dimensionless natural frequency of a moderately thick sandwich panel. It is shown that the porous core type 2, followed by porous core type 1, and then the uniform core, have the highest dimensionless natural frequency, respectively. Additionally, the core with a ratio of $h_c/h_f = 6-8$ has the highest dimensionless natural frequency.

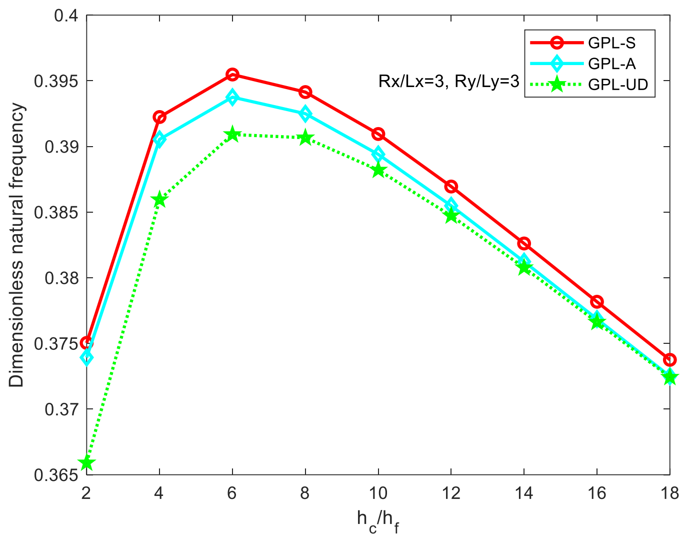

Fig. 3: The effect of different distribution of graphene platelets on dimensionless natural frequency of sandwich panel

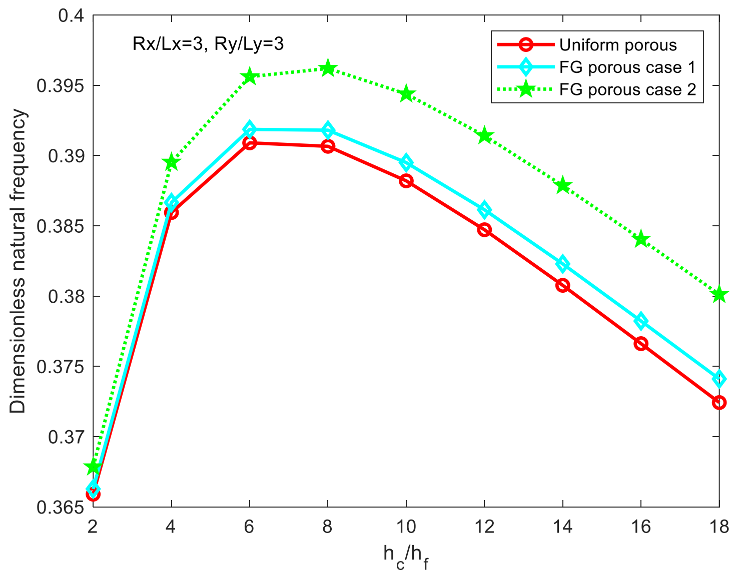

Fig. 4: The effect of various porosity distributions including uniform distribution on dimensionless natural frequency sandwich panel

Fig. 5 illustrates the graph of different volume fractions of graphene platelets, showing that as the volume fraction of the graphene layers increases, the dimensionless natural frequency also increases, because the stiffness of the sandwich panel enhances. The highest dimensionless natural frequency occurs at the ratio of $h_c/h_f = 6$

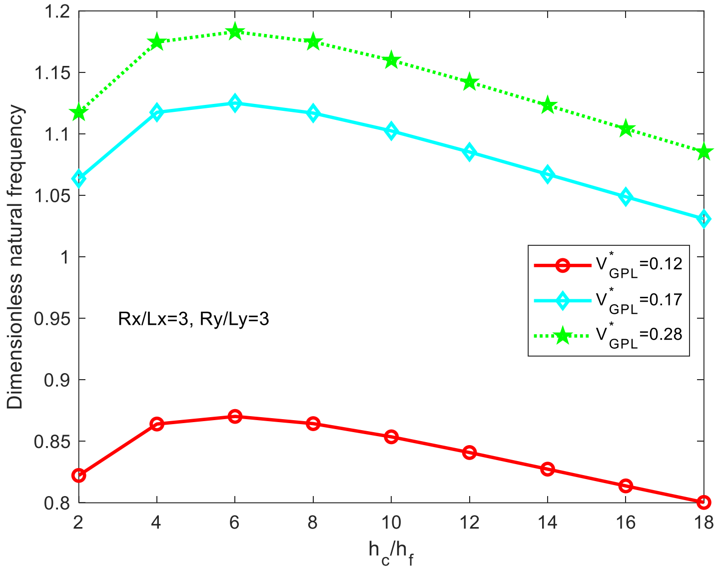

Fig. 5: The dimensionless natural frequency of the sandwich panel for different volume fraction of graphene platelets

Fig. 6 shows the effect of magnetic and electric fields, where the combination of both magnetic and electric fields results in the highest dimensionless natural frequency. In contrast, when neither field is applied, the lowest dimensionless natural frequency is observed. In this case $V_0 = 1.5V$, $\Psi_0 = 12.5\ A$, the effect of the magnetic field is greater than that of the electric field.

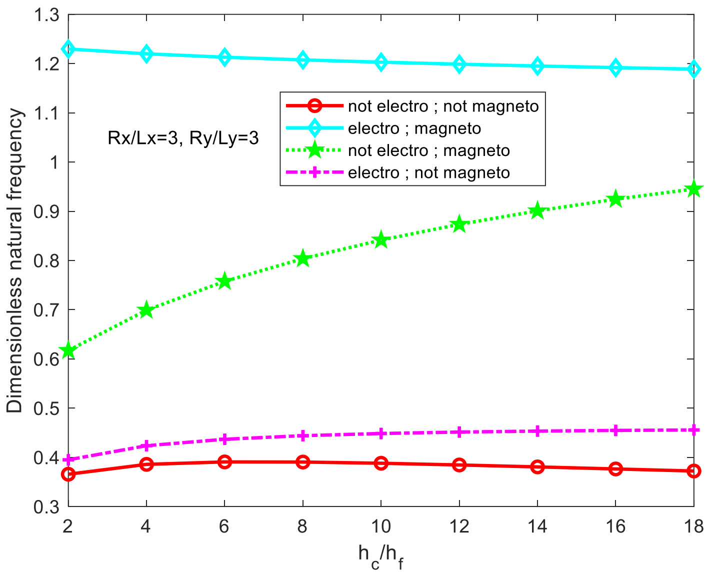

Fig. 6: The effect of magnetic and electric fields on dimensionless natural frequency sandwich panel

3. Conclusion

In previous studies, researchers have focused on the vibrational behavior of double-curved sandwich shell panels. In contrast, the present study concentrates on the vibration analysis of a moderately thick double-curved sandwich panels with a porous core reinforced and graphene platelets reinforced composite face sheets. This analysis is based on the first-order shear deformation theory and the non-local strain gradient theory, which are widely used in various industries including marine, military, and construction industries. The results obtained by research of Sayyad and Ghugal [50] are validated that there is a good agreement between them. Moreover, because increasing high strength to weight in the double-curved sandwich panel, these structures are used. The obtained results of this research can be listed as follows:

- The dimensionless natural frequency for a cylindrical panel with a porous core and graphene sheets is higher than that of a spherical panel
- For the spherical panel, the dimensionless natural frequency is directly related to the curvature radius of sphere; however, there is an inverse result for the cylindrical panel.
- The symmetric graphene platelets in face sheet layers has the highest dimensionless natural frequency, rather than the asymmetric and uniform graphene platelets.
- The highest dimensionless natural frequency is occurred for the porous core type 2, and then followed by porous core type 1, and the uniform core.
- The dimensionless natural frequency increases with increasing the volume fraction of the graphene platelet, because the stiffness of a moderately thick sandwich panel.
- Magnetic and electric fields have a significant impact on double-curved sandwich panels. Also, it is shown that the effect of the magnetic field is greater than that of the electric field.
- As the figures show, in $h_c/h_f = 6$ the dimensionless natural frequency has the highest value, which can be considered in the design of thick double-curved sandwich panels.

Declaration of Competing Interest

No conflict of interest exists in the submission of this article, and all authors approve the article for publication.

Acknowledgments

The authors appreciate the referees for their valuable comments and express gratitude for their impact on improving the quality of this paper.

References

[1] M. Kholdi, G. Rahimi, A. Loghman, H. Ashrafi, M. Arefi, Analysis of thick spherical shells subjected to various temperature gradients: thermo-elasto-plastic and residual stress studies, *International Journal of Applied Mechanics,* Vol. 13, No. 9, pp. 2150105, 2021.

[2] E. Sobhani, Vibrational characteristics of fastening of a spherical shell with a coupled conical-conical shells strengthened with nanocomposite sandwiches contained agglomerated CNT face layers and GNP core under spring boundary conditions, *Engineering Analysis with Boundary Elements,* Vol. 146, No. 10, pp. 362-387, 2023.

[3] E. Sobhani, A. R. Masoodi, A. R. Ahmadi-Pari, Circumferential vibration analysis of nano-porous-sandwich assembled spherical-cylindrical-conical shells under elastic boundary conditions, *Engineering Structures,* Vol. 273, No. 27, pp. 115094, 2022.

[4] S. Wang, S. Lin, A novelly universal theory: Toward accurately evaluating radial vibration characteristics for radially sandwiched spherical piezoelectric transducer, *Ultrasonics,* Vol. 111, No. 2, pp. 106299, 2021.

[5] R. K. Yadav, S. S. Gupta, Inextensional vibrations of thin spherical shells using strain gradient elasticity theory, *Thin-Walled Structures,* Vol. 202, No. 15-16, pp. 112061, 2024.

[6] J. Liu, J. Lou, K. Chai, Q. Yang, Nonlinear vibration-acoustic analysis of the coupled system of flexible cylindrical shell foundation and HSLDS vibration isolator, *Thin-Walled Structures,* Vol. 209, pp. 112896, 2025.

[7] L. Wang, D. Cao, J. Gu, Nonlinear stochastic vibration of GPRMF cylindrical shell with harmonic and white noise excitations, *Communications in Nonlinear Science and Numerical Simulation,* Vol. 142, pp. 108592, 2025.

[8] C. Kai, L. Junfeng, L. Jingiun, L. Shuyong, Vibration characteristics of cylindrical shells with discontinuous connections based on the spectral element method, *International Journal of Solids and Structures,* Vol. 308, pp. 113148, 2024.

[9] S. Zhang, L. Ding, X. Wu, Y. Ma, Z. Deng, Broadband vibration reduction of cylindrical shell structures with circumferential taper scatters, *Journal of Sound and Vibration,* Vol. 599, pp. 118853, 2024.

[10] P. T. Thang, C. Kim, H. Jang, T. Kim, J. Kim, Free vibration characteristics of honeycomb sandwich cylindrical shells reinforced with graphene nanoplatelets/polymer coatings, *Aerospace Science and Technology,* Vol. 156, pp. 109744, 2024.

[11] M. Khorasani, Z. Soleimani-Javid, E. Arshid, S. Amir, O. Civalek, Vibration analysis of graphene nanoplatelets' reinforced composite plates integrated by piezo-electromagnetic patches on the piezo-electromagnetic media, *Waves in Random and Complex Media,* Vol. 34, No. 4, pp. 2394-2424, 2021.

[12] J. Kargar, A. Ghorbanpour Arani, E. Arshid, M. Irani Rahaghi, Vibration analysis of spherical sandwich panels with MR fluids core and magneto-electro-elastic face sheets resting on orthotropic viscoelastic foundation, *Structural Engineering and Mechanics,* Vol. 78, No. 5, pp. 557-572, 2021.

[13] M. Mahinzare, A. Rastgoo, F. Ebrahimi, Magnetic field effects on wave dispersion of piezo-electrically actuated auxetic sandwich shell via GPL reinforcement, *Journal of the Brazilian Society of Mechanical Sciences and Engineering,* Vol. 46, No. 2, pp. 102-148, 2024.

[14] Q. H. Pham, V. K. Tran, P. C. Nguyen, Nonlocal refined higher isogeometric analysis for vibration characteristics of porous metal foam magneto-electro-elastic curved nanobeam with elastic boundary conditions, *Engineering Science and Technology, an International Journal,* Vol. 54, pp. 101715, 2024.

[15] R. Rostami, M. Mohammadimehr, Vibration control of rotating sandwich cylindrical shell-reinforced nanocomposite face sheet and porous core integrated with functionally graded magneto-electro-elastic layers, *Engineering with Computers,* Vol. 38, No. 1, pp. 87-100, 2022.

[16] E. Arshid, S. Amir, A. Loghman, Thermoelastic vibration characteristics of asymmetric annular porous reinforced with nano-fillers microplates embedded in an elastic medium: CNTs Vs. GNPs, *Archives of Civil and Mechanical Engineering,* Vol. 23, No. 2, 2023.

[17] A. Ebrahimi-Mamaghani, O. Koochakianfard, M. Rafiei, A. Alibeigloo, A. Satary Dizaji, V. Borjalilou, Machine learning, analytical, and numerical techniques for vibration analysis of submerged porous functional gradient piezoelectric microbeams with movable supports, *International Journal of Structural Stability and Dynamics*, 2024.

[18] A. Ghorbanpour Arani, M. Pakize, M. Irani Rahaghi, Z. Khoddami Maraghi, S. Niknejad, Vibrational Study on Multilayer Sandwich Plates: Porous FGM Core, Nanocomposite and Piezoelectric Face Sheets, *Journal of Solid Mechanics,* Vol. 16, No. 3, 2024.

[19] J. Chen, J. Wu, J. Chen, Vortex induced vibration control of a cactus-shaped cylinder with porous spines, *Ocean Engineering,* Vol. 313, No. 1, pp. 119401, 2024.

[20] C. Ying, G. Guan, G. Liang, Q. Yang, Numerical investigation on flow-induced vibration of porous square cylinder and its mechanism research, *Ocean Engineering,* Vol. 309, No. 1, pp. 118314, 2024.

[21] M. A. Mohammadimehr, A. Loghman, S. Amir, M. Mohammadimehr, E. Arshid, Vibration behavior of a thick double-curved sandwich panel with porous core and carbon nanotube reinforced composite based on TSDDCT and NSGT, *Acta Mechanica*, pp. 1-34, 2025.

[22] Q. Wu, M. Yao, Y. Niu, Nonplanar free and forced vibrations of an imperfect nanobeam employing nonlocal strain gradient theory, *Communications in Nonlinear Science and Numerical Simulation,* Vol. 114, pp. 106692, 2022.

[23] H. Babaei, M. R. Eslami, Nonlinear analysis of thermal-mechanical coupling bending of FGP infinite length cylindrical panels based on PNS and NSGT, *Applied Mathematical Modelling,* Vol. 91, No. 12, pp. 1061-1080, 2021.

[24] B. Marinca, N. Herisanu, V. Marinca, Investigating nonlinear forced vibration of functionally graded nanobeam based on the nonlocal strain gradient theory considering mechanical impact, electromagnetic actuator, thickness effect and nonlinear foundation, *European Journal of Mechanics - A/Solids,* Vol. 102, No. 2, pp. 105119, 2023.

[25] M. Mohammadian, S. M. Hosseini, A. Mohamad, A size-dependent differential quadrature element model for vibration analysis of FG CNT reinforced composite microrods based on the higher order Love-Bishop rod model and the nonlocal strain gradient theory, *Engineering Analysis with Boundary Elements,* Vol. 138, pp. 235-252, 2022.

[26] H. R. Moghaddasi, M. Azhari, M. M. Saadatpour, S. Sarrami, Large-amplitude vibrations of thick cantilevered circular cylindrical shells containing still fluid, *Journal of Fluids and Structures,* Vol. 115, No. 1, pp. 103784, 2022.

[27] M. Vazirzadeh, J. Rouzegar, M. H. Heydari, A refined fractional viscoelastic model for vibration analysis of moderately-thick plates, *Mechanics Research Communications,* Vol. 135, No. 22-23, pp. 104224, 2024.

[28] Z. Hu, Z. Ni, D. An, Y. Chen, R. Li, Hamiltonian system-based analytical solutions for the free vibration of edge-cracked thick rectangular plates, *Applied Mathematical Modelling,* Vol. 117, No. 5, pp. 451-478, 2023.

[29] J. Li, G. Kardomateas, L. Liu, Vibration analysis of thick-section sandwich structures in thermal environments, *International Journal of Mechanical Sciences,* Vol. 241, No. 7, pp. 107937, 2023.

[30] C. C. Hong, GDQ computation for thermal vibration of thick FGM plates by using third-order shear deformation theory, *Materials Science and Engineering: B,* Vol. 294, pp. 116208, 2023.

[31] R. Zhong, T. Liu, Q. Wang, *5-Free and forced vibrations of functionally graded porous shallow shells on elastic foundation*, in: *Machine Learning Aided Analysis, Design, and Additive Manufacturing of Functionally Graded Porous Composite Structures*, Eds., pp. 139-172, 2024.

[32] A. H. Sofiyev, F. Turan, On the nonlinear vibration of heterogenous orthotropic shallow shells in the framework of the shear deformation shell theory, *Thin-Walled Structures,* Vol. 161, No. 3, pp. 107181, 2021.

[33] H. Babaei, Free vibration and snap-through instability of FG-CNTRC shallow arches supported on nonlinear elastic foundation, *Applied Mathematics and Computation,* Vol. 413, pp. 126606, 2022.

[34] A. Kumar, D. Kumar, Vibration analysis of functionally graded stiffened shallow shells under thermo-mechanical loading, *Materials Today: Proceedings,* Vol. 44, No. 6, pp. 4590-4595, 2022.

[35] A. M. Dehrouyeh-Semnani, H. Mostafaei, Vibration analysis of scale-dependent thin shallow microshells with arbitrary planform and boundary conditions, *International Journal of Engineering Science,* Vol. 158, pp. 103413, 2021.

[36] M. Mohammadimehr, M. A. Mohammadimehr, P. Dashti, Size-dependent effect on biaxial and shear nonlinear buckling analysis of nonlocal isotropic and orthotropic micro-plate based on surface stress and modified couple stress, *Applied Mathematics and Mechanics,* Vol. 37, No. 4, pp. 529-554, 2016.

[37] A. S. Khalaf, H. M. Hasan, Nonlinear forced vibration of functionally graded hybrid three-phase nanocomposite toroidal shell segments reinforced by carbon nanotubes (CNTs) and graphene nanoplatelets (GPLs), *Thin-Walled Structures,* Vol. 199, pp. 111876, 2024.

[38] M. Mirzaei, R. Rabiei, On the free and forced vibrations of porous GPL reinforced composite conical panels using a Legendre-Ritz method, *Engineering Analysis with Boundary Elements,* Vol. 163, No. 3879, pp. 378-393, 2024.

[39] Z. Feng, X. Yang, H. Keshavarzpour, A. Ghasemi, Free vibration analysis of hybrid CNT/GPL-reinforced Porous composite plates under fluid-loading, *Aerospace Science and Technology,* Vol. 148, No. 10, pp. 109116, 2024.

[40] F. Bargozini, M. Mohammadimehr, E. A. Dawi, M. Salavati-Niasari, Buckling of a sandwich beam with carbon nano rod reinforced composite and porous core under axially variable forces by considering general strain, *Results in Engineering,* Vol. 21, No. 5, pp. 101945, 2024.

[41] M. Bamdad, M. Mohammadimehr, K. Alambeigi, Analysis of sandwich Timoshenko porous beam with temperature-dependent material properties: Magneto-electro-elastic vibration and buckling solution, *Journal of Vibration and Control,* Vol. 0, No. 0, pp. 1-19, 2019.

[42] M. Pahlavanzadeh, M. Mohammadimehr, M. Irani-Rahaghi, S. M. Emamat, Vibration response on the rod of vortex bladeless wind power generator for a sandwich beam with various face sheets and cores based on different boundary conditions, *Mechanics Based Design of Structures and Machines,* Vol. 53, No. 3, pp. 1709-1735, 2025.

[43] O. Rahmani, S. M. R. Khalili, O. T. Thomsen, A high-order theory for the analysis of circular cylindrical composite sandwich shells with transversely compliant core subjected to external loads, *Composite Structures,* Vol. 94, No. 7, pp. 2129-2142, 2012.

[44] T. Kant, D. Punera, A Refined Higher Order Theory for Statics and Dynamics of Doubly Curved Shells, *Indian National Science Academy,* Vol. 83, No. 1, pp. 611-630, 2017.

[45] E. Arshid, A. Kiani, S. Amir, M. Zarghami Dehaghani, Asymmetric free vibration analysis of first-order shear deformable functionally graded magneto-electro-thermo-elastic circular plates, *Journal of Mechanical Engineering Science,* Vol. 0, No. 0, pp. 1-17, 2019.

[46] D. Punera, T. Kant, Elastostatics of laminated and functionally graded sandwich cylindrical shells with two refined higher order models, *Composite Structures,* Vol. 182, pp. 505-523, 2017.

[47] Q. H. Pham, V. K. Tran, P. C. Nguyen, Dynamic response of magneto-electro-elastic composite plates lying on visco-Pasternak medium subjected to blast load, *Composite Structures,* Vol. 337, pp. 118054, 2024.

[48] M. Mohammadimehr, M. Mostafavifar, Free vibration analysis of sandwich plate with a transversely flexible core and FG-CNTs reinforced nanocomposite face sheets subjected to magnetic field and temperature-dependent material properties using SGT, *Composites Part B Engineering,* Vol. 94, pp. 253-270, 2016.

[49] C. Liu, L. L. Ke, Y. S. Wang, J. Yang, S. Kitipornchai, Thermo-electro-mechanical vibration of piezoelectric nanoplates based on the nonlocal theory, *Composite Structures,* Vol. 106, pp. 167-174, 2013.

[50] A. S. Sayyad, Y. M. Ghugal, Static and free vibration analysis of doubly-curved functionally graded material shells, *Composite Structures,* Vol. 269, pp. 114045, 2021.

Appendix A. The stiffness coefficients

The stiffness coefficients of a double-curved moderately thick sandwich panel with a porous core and nanocomposite tops reinforced with GPLs are considered as follows:

$$Q_{11}^{*\mathrm{yxz}(i)} = \int_{-h_b-h_c/2}^{-h_c/2} \mathrm{A}_{yx}\, Q_{11}^{(b)} z^i dz + \int_{-h_c/2}^{h_c/2} \mathrm{A}_{yx}\, Q_{11}^{(\mathrm{c})} z^i dz + \int_{h_c/2}^{h_c/2+h_t} \mathrm{A}_{yx}\, Q_{11}^{(\mathrm{t})} z^i dz \quad i = 0,1,2,3,4,6$$

$$Q_{12}^{*0\mathrm{z}(i)} = \int_{-h_b-h_c/2}^{-h_c/2} \mathrm{A}_0 Q_{12}^{(b)} z^i dz + \int_{-h_c/2}^{h_c/2} \mathrm{A}_0 Q_{12}^{(\mathrm{c})} z^i dz + \int_{h_c/2}^{h_c/2+h_t} \mathrm{A}_0 Q_{12}^{(\mathrm{t})} z^i dz \quad i = 0,1,2,3,4,6$$

$$Q_{22}^{*xy\,\mathrm{z}(i)} = \int_{-h_b-h_c/2}^{-h_c/2} \mathrm{A}_{xy}\, Q_{22}^{(b)} z^i dz + \int_{-h_c/2}^{h_c/2} \mathrm{A}_{xy}\, Q_{22}^{(\mathrm{c})} z^i dz + \int_{h_c/2}^{h_c/2+h_t} \mathrm{A}_{xy}\, Q_{22}^{(\mathrm{t})} z^i dz \quad i = 0,1,2,3,4,6$$

$$Q_{44}^{*0\mathrm{z}(i)} = \int_{-h_b-h_c/2}^{-h_c/2} \mathrm{A}_0 Q_{44}^{(b)} z^i dz + \int_{-h_c/2}^{h_c/2} \mathrm{A}_0 Q_{44}^{(\mathrm{c})} z^i dz + \int_{h_c/2}^{h_c/2+h_t} \mathrm{A}_0 Q_{44}^{(\mathrm{t})} z^i dz \quad i = 2,4,6$$

$$Q_{44}^{*xy\,\mathrm{z}(i)} = \int_{-h_b-h_c/2}^{-h_c/2} \mathrm{A}_{xy}\, Q_{44}^{(b)} z^i dz + \int_{-h_c/2}^{h_c/2} \mathrm{A}_{xy}\, Q_{44}^{(\mathrm{c})} z^i dz + \int_{h_c/2}^{h_c/2+h_t} \mathrm{A}_{xy}\, Q_{44}^{(\mathrm{t})} z^i dz \quad i = 2,4,6$$

$$Q_{44}^{*yx\,\mathrm{z}(i)} = \int_{-h_b-h_c/2}^{-h_c/2} \mathrm{A}_{yx}\, Q_{44}^{(b)} z^i dz + \int_{-h_c/2}^{h_c/2} \mathrm{A}_{yx}\, Q_{44}^{(\mathrm{c})} z^i dz + \int_{h_c/2}^{h_c/2+h_t} \mathrm{A}_{yx}\, Q_{44}^{(\mathrm{t})} z^i dz \quad i = 2,4,6$$

$$Q_{44}^{*0\mathrm{z}(i)} = \int_{-h_b-h_c/2}^{-h_c/2} \mathrm{A}_0 Q_{44}^{(b)} z^i dz + \int_{-h_c/2}^{h_c/2} \mathrm{A}_0 Q_{44}^{(\mathrm{c})} z^i dz + \int_{h_c/2}^{h_c/2+h_t} \mathrm{A}_0 Q_{44}^{(\mathrm{t})} z^i dz \quad i = 2,4,6 \qquad \text{(A-1)}$$

$$Q_{55}^{*y\,\mathrm{z}(i)} = \int_{-h_b-h_c/2}^{-h_c/2} \mathrm{A}_y\, Q_{55}^{(b)} z^i dz + \int_{-h_c/2}^{h_c/2} \mathrm{A}_y\, Q_{55}^{(\mathrm{c})} z^i dz + \int_{h_c/2}^{h_c/2+h_t} \mathrm{A}_y\, Q_{55}^{(\mathrm{t})} z^i dz \quad i = 0,1,2,3,5$$

$$Q_{55}^{*yx\,\mathrm{z}(i)} = \int_{-h_b-h_c/2}^{-h_c/2} \mathrm{A}_{yx}\, Q_{55}^{(b)} z^i dz + \int_{-h_c/2}^{h_c/2} \mathrm{A}_{yx}\, Q_{55}^{(\mathrm{c})} z^i dz + \int_{h_c/2}^{h_c/2+h_t} \mathrm{A}_{yx}\, Q_{55}^{(\mathrm{t})} z^i dz \quad i = 0,1,2,3,4,6$$

$$Q_{55}^{*xmy\,\mathrm{z}(i)} = \int_{-h_b-h_c/2}^{-h_c/2} \mathrm{A}_{xmy}\, Q_{55}^{(b)} z^i dz + \int_{-h_c/2}^{h_c/2} \mathrm{A}_{xmy}\, Q_{55}^{(\mathrm{c})} z^i dz + \int_{h_c/2}^{h_c/2+h_t} \mathrm{A}_{xmy}\, Q_{55}^{(\mathrm{t})} z^i dz \quad i = 0,2,4$$

$$Q_{66}^{*x\,\mathrm{z}(i)} = \int_{-h_b-h_c/2}^{-h_c/2} \mathrm{A}_x\, Q_{66}^{(b)} z^i dz + \int_{-h_c/2}^{h_c/2} \mathrm{A}_x\, Q_{66}^{(\mathrm{c})} z^i dz + \int_{h_c/2}^{h_c/2+h_t} \mathrm{A}_x\, Q_{66}^{(\mathrm{t})} z^i dz \quad i = 0,1,2,3,5$$

$$Q_{66}^{*xy\,\mathrm{z}(i)} = \int_{-h_b-h_c/2}^{-h_c/2} \mathrm{A}_{xy}\, Q_{66}^{(b)} z^i dz + \int_{-h_c/2}^{h_c/2} \mathrm{A}_{xy}\, Q_{66}^{(\mathrm{c})} z^i dz + \int_{h_c/2}^{h_c/2+h_t} \mathrm{A}_{xy}\, Q_{66}^{(\mathrm{t})} z^i dz \quad i = 0,1,2,3,4,6$$

$$Q_{66}^{*xmy\,\mathrm{z}(i)} = \int_{-h_b-h_c/2}^{-h_c/2} \mathrm{A}_{xmy}\, Q_{66}^{(b)} z^i dz + \int_{-h_c/2}^{h_c/2} \mathrm{A}_{xmy}\, Q_{66}^{(\mathrm{c})} z^i dz + \int_{h_c/2}^{h_c/2+h_t} \mathrm{A}_{xmy}\, Q_{66}^{(\mathrm{t})} z^i dz \quad i = 0,2,4$$

where the coefficients are defined as:

$$
\begin{aligned}
&A_0 = 1 \\
&A_k = 1 + z/R_k \\
&A_{kl} = (1 + z/R_k)/(1 + z/R_l) \\
&A_{kml} = (1 + z/R_k)(1 + z/R_l) \\
&A^*_{kml} = (1 + z/R_k)(1 + z/R_l)\cos\left(\frac{\pi z}{h}\right)
\end{aligned}
\tag{A-2}
$$

Appendix B. The mass moment of inertia

The coefficients of the mass moment of inertia for the sandwich panel are calculated as follows:

$$
I^{*i} = \int_{-h_b - h_c/2}^{-h_c/2} \mathrm{A}_{xmy}\ \rho^{(b)} z^{\,i} dz + \int_{-h_c/2}^{h_c/2} \mathrm{A}_{xmy}\ \rho^{(c)} z^{\,i} dz + \int_{h_c/2}^{h_c/2 + h_t} \mathrm{A}_{xmy}\ \rho^{(t)} z^{\,i} dz \quad i = 0,1,2,3,4,6
\tag{B}
$$

Appendix C. The governing equations of motion for a double-curved, thick sandwich panel

Assuming the following equations and placing the resulting forces and moments in the equations of motion, the governing equations of motion for a double-curved thick sandwich panel with porous core and anocomposite face sheets reinforced by GPL based on first-order shear deformation double-curved theory (FSDT) and NSGT are calculated as follows:

$$
\alpha_m = \frac{m\,\pi}{L_x} \quad , \quad \beta_n = \frac{n\,\pi}{L_y}
\tag{C-1}
$$

$$
\begin{aligned}
&(1 - l_m^2 \nabla^2)\{a_{11} u + a^*_{11} \frac{\partial^2 u}{\partial x^2} + a^{**}_{11} \frac{\partial^2 u}{\partial y^2} + a_{12} \frac{\partial^2 v}{\partial x\, \partial y} + a_{13} \frac{\partial w}{\partial x} + a^*_{13} \frac{\partial^3 w}{\partial x^3} + a^{**}_{13} \frac{\partial^3 w}{\partial x\, \partial y^2} \\
&+ a_{14}\, \phi_{\mathrm{x}} + a^*_{14} \frac{\partial^2 \phi_{\mathrm{x}}}{\partial x^2} + a^{**}_{14} \frac{\partial^2 \phi_{\mathrm{x}}}{\partial y^2} + a_{15} \frac{\partial^2 \phi_y}{\partial x\, \partial y} + a_{16} \frac{\partial \phi}{\partial x} + a_{17} \frac{\partial \psi}{\partial x}\} \\
&+ [1 - (e_0 a)^2 \nabla^2]\{I^{*0} \frac{\partial^2 u}{\partial t^2} + I^{*1} \frac{\partial^2 \phi_x}{\partial t^2}\} = 0
\end{aligned}
\tag{C-2}
$$

$$
\begin{aligned}
&(1 - l_m^2 \nabla^2)\{a_{21} \frac{\partial^2 u}{\partial x \partial y} + a_{22} v + a^*_{22} \frac{\partial^2 v}{\partial x^2} + a^{**}_{22} \frac{\partial^2 v}{\partial y^2} + a_{23} \frac{\partial w}{\partial y} + a^*_{23} \frac{\partial^3 w}{\partial y^3} + a^{**}_{23} \frac{\partial^3 w}{\partial x^2 \partial y} + a_{24} \frac{\partial^2 \phi_x}{\partial x \partial y} \\
&+ a_{25}\, \phi_y + a^*_{25} \frac{\partial^2 \phi_y}{\partial x^2} + a^{**}_{25} \frac{\partial^2 \phi_y}{\partial y^2} + a_{26} \frac{\partial \phi}{\partial y} + a_{27} \frac{\partial \psi}{\partial y}\} + [1 - (e_0 a)^2 \nabla^2]\{I^{*0} \frac{\partial^2 v}{\partial t^2} + I^{*1} \frac{\partial^2 \phi_y}{\partial t^2}\} = 0
\end{aligned}
\tag{C-3}
$$

$$(1-l_m^2\nabla^2)\{-a_{31}\frac{\partial u}{\partial x}-a_{31}^{*}\frac{\partial^3 u}{\partial x^3}-a_{31}^{**}\frac{\partial^3 u}{\partial x\,\partial y^2}-a_{32}\frac{\partial v}{\partial y}-a_{32}^{*}\frac{\partial^3 v}{\partial y^3}-a_{32}^{**}\frac{\partial^3 v}{\partial x^2\partial y}+a_{33}w$$
$$+a_{33}^{*}\frac{\partial^2 w}{\partial x^2}+a_{33}^{**}\frac{\partial^2 w}{\partial y^2}+a_{33}^{***}\frac{\partial^4 w}{\partial x^2\partial y^2}+a_{33}^{2*}\frac{\partial^4 w}{\partial x^4}+a_{33}^{2**}\frac{\partial^4 w}{\partial y^4}+a_{34}\frac{\partial \phi_x}{\partial x}+a_{34}^{*}\frac{\partial^3 \phi_x}{\partial x^3}$$
$$+a_{34}^{**}\frac{\partial^3 \phi_x}{\partial x\,\partial y^2}+a_{35}\frac{\partial \phi_y}{\partial y}+a_{35}^{*}\frac{\partial^3 \phi_y}{\partial y^3}+a_{35}^{**}\frac{\partial^3 \phi_y}{\partial x^2\partial y}-a_{36}\phi-a_{37}\psi\}$$
$$+[1-(e_0a)^2\nabla^2]\{I^{*0}\frac{\partial^2 w}{\partial t^2}\}=0 \tag{C-4}$$

$$(1-l_m^2\nabla^2)\{a_{41}u+a_{41}^{*}\frac{\partial^2 u}{\partial x^2}+a_{41}^{**}\frac{\partial^2 u}{\partial y^2}+a_{42}\frac{\partial^2 v}{\partial x\,\partial y}-a_{43}\frac{\partial w}{\partial x}-a_{43}^{*}\frac{\partial^3 w}{\partial x^3}-a_{43}^{**}\frac{\partial^3 w}{\partial x\,\partial y^2}$$
$$+a_{44}\phi_{\mathrm{x}}+a_{44}^{*}\frac{\partial^2 \phi_{\mathrm{x}}}{\partial x^2}+a_{44}^{**}\frac{\partial^2 \phi_{\mathrm{x}}}{\partial y^2}+a_{45}\frac{\partial^2 \phi_y}{\partial x\,\partial y}+a_{46}\frac{\partial \phi}{\partial x}+a_{47}\frac{\partial \psi}{\partial x}\}$$
$$+[1-(e_0a)^2\nabla^2]\{I^{*1}\frac{\partial^2 u}{\partial t^2}+I^{*2}\frac{\partial^2 \phi_x}{\partial t^2}\}=0 \tag{C-5}$$

$$(1-l_m^2\nabla^2)\{a_{51}\frac{\partial^2 u}{\partial x\,\partial y}+a_{52}v+a_{52}^{*}\frac{\partial^2 v}{\partial x^2}+a_{52}^{**}\frac{\partial^2 v}{\partial y^2}-a_{53}\frac{\partial w}{\partial y}-a_{53}^{*}\frac{\partial^3 w}{\partial y^3}-a_{53}^{**}\frac{\partial^3 w}{\partial x^2\partial y}$$
$$+a_{54}\frac{\partial^2 \phi_x}{\partial x\,\partial y}+a_{55}\phi_y+a_{55}^{*}\frac{\partial^2 \phi_y}{\partial x^2}+a_{55}^{**}\frac{\partial^2 \phi_y}{\partial y^2}+a_{56}\frac{\partial \phi}{\partial y}+a_{57}\frac{\partial \psi}{\partial y}\}$$
$$+[1-(e_0a)^2\nabla^2]\{I^{*1}\frac{\partial^2 v}{\partial t^2}+I^{*2}\frac{\partial^2 \phi_y}{\partial t^2}\}=0 \tag{C-6}$$

$$(1-l_m^2\nabla^2)\{-a_{16}\frac{\partial u}{\partial x}-a_{26}\frac{\partial v}{\partial y}-a_{36}w-a_{46}\frac{\partial \phi_{\mathrm{x}}}{\partial x}-a_{56}\frac{\partial \phi_y}{\partial y}+a_{66}\phi+a_{67}\psi\}=0 \tag{C-7}$$

$$(1-l_m^2\nabla^2)\{-a_{17}\frac{\partial u}{\partial x}-a_{27}\frac{\partial v}{\partial y}-a_{37}w-a_{47}\frac{\partial \phi_{\mathrm{x}}}{\partial x}-a_{57}\frac{\partial \phi_y}{\partial y}+a_{67}\phi+a_{77}\psi\}=0 \tag{C-8}$$

where the coefficients of $a_{ij}=a_{ji}, a_{ij}^{*}=a_{ji}^{*}, a_{ij}^{**}=a_{ji}^{**}, i,j=1,2,3,4,5,6,7$ in Eqs. (D-1) and (D-2) are defined as follows:

$$a_{11}=Q_{55}^{*yxz(0)}\frac{1}{R_x^2}\quad,\quad a_{11}^{*}=-Q_{11}^{*yxz(0)}\quad,\quad a_{11}^{**}=-Q_{44}^{*xyz(0)}\quad,\quad a_{12}=-Q_{12}^{*0z(0)}-Q_{44}^{*0z(0)}$$
$$a_{13}=-Q_{11}^{*yxz(0)}\frac{1}{R_x}-Q_{12}^{*0z(0)}\frac{1}{R_y}-Q_{55}^{*yxz(0)}\frac{1}{R_x}\quad,\quad a_{13}^{*}=-Q_{11}^{*1yxz(3)}c_1^{*}-Q_{11}^{*yxz(6)}c_1^{*2}\frac{(\alpha_1-1)}{R_x}\quad,\quad a_{13}^{**}=0$$
$$a_{14}=-Q_{55}^{*yz(0)}\frac{1}{R_x}+Q_{55}^{*yxz(1)}\frac{1}{R_x^2}, a_{14}^{*}=-Q_{11}^{*1yxz(1)}, a_{14}^{**}=-Q_{44}^{*xyz(1)},$$
$$a_{15}=-Q_{12}^{*0z(1)}-Q_{44}^{*0z(1)}, a_{16}=e_{31}A_{yx}^{z(0)}\frac{1}{R_x} \tag{C-9}$$

$$a_{17} = f_{31} A_{yx}^{z(0)} \frac{1}{R_x},\ a_{22} = Q_{66}^{*xyz(0)} \frac{1}{R_y^2},\ a_{22}^{*} = -Q_{44}^{*xyz(0)},\ a_{22}^{**} = -Q_{22}^{*xyz(0)},$$

$$a_{23}^{*} = 0 \quad , \quad a_{23}^{**} = 0$$

$$a_{23} = -Q_{12}^{*0z(0)} \frac{1}{R_x} - Q_{22}^{*xyz(0)} \frac{1}{R_y} - Q_{66}^{*xyz(0)} \frac{1}{R_y} \quad , \quad a_{24} = -Q_{12}^{*0z(1)} - Q_{44}^{*0z(1)}$$

$$a_{25} = -Q_{66}^{*xz(0)} \frac{1}{R_y} + Q_{66}^{*xyz(1)} \frac{1}{R_y^2} \quad , \ a_{25}^{*} = -Q_{44}^{*yxz(1)} \quad , \quad a_{25}^{**} = -Q_{22}^{*xyz(1)},\ a_{26} = e_{31} A_{xy}^{z(0)} \frac{1}{R_y}$$

$$a_{27} = f_{31} A_{xy}^{z(0)} \frac{1}{R_y} \quad , \quad a_{33}^{*} = -Q_{55}^{*yxz(0)} \quad , \quad a_{33}^{**} = -Q_{66}^{*xyz(0)} \quad , \quad a_{33}^{***} = 0 \quad , \quad a_{33}^{2*} = 0 \quad , \quad a_{33}^{2**} = 0$$

$$a_{33} = Q_{11}^{*yxz(0)} \frac{1}{R_x^2} + 2Q_{12}^{*0z(0)} \frac{1}{R_x R_y} + Q_{22}^{*xyz(0)} \frac{1}{R_y^2} \quad , \quad a_{34}^{*} = 0 \quad , \quad a_{34}^{**} = 0 \quad , \quad a_{35}^{*} = 0$$

$$a_{34} = Q_{11}^{*yxz(1)} \frac{1}{R_x} + Q_{12}^{*0z(1)} \frac{1}{R_y} - Q_{55}^{*yz(0)} + Q_{55}^{*yxz(1)} \frac{1}{R_x} \quad ,$$

$$a_{35} = Q_{12}^{*0z(1)} \frac{1}{R_x} + Q_{22}^{*xyz(1)} \frac{1}{R_y} + Q_{66}^{*xyz(1)} \frac{1}{R_y} - Q_{66}^{*xz(0)}$$

$$a_{35}^{**} = 0 \quad , \quad a_{36} = e_{31} A_{yx}^{z(0)} \frac{1}{R_x^2} + e_{31} A_{xy}^{z(0)} \frac{1}{R_y^2} \quad , \quad a_{37} = f_{31} A_{yx}^{z(0)} \frac{1}{R_x^2} + f_{31} A_{xy}^{z(0)} \frac{1}{R_y^2},$$

$$a_{44}^{*} = -Q_{11}^{*yxz(2)}$$

$$a_{44}^{**} = -Q_{44}^{*xyz(2)} \quad , \quad a_{44} = Q_{55}^{*xmyz(0)} - 2Q_{55}^{*yz(1)} \frac{1}{R_x} + Q_{55}^{*yxz(2)} \frac{1}{R_x^2} \quad ,$$

$$a_{45} = -Q_{12}^{*0z(2)} - Q_{44}^{*0z(2)} - Q_{44}^{*0z(4)}$$

$$a_{46} = e_{31} A_{yx}^{z(1)} \frac{1}{R_x} - e_{31} A_{y}^{z(0)} \quad , \quad a_{47} = f_{31} A_{yx}^{z(1)} \frac{1}{R_x} - f_{31} A_{y}^{z(0)} \ ,$$

$$a_{55}^{*} = -Q_{44}^{*yxz(2)} \quad , \quad a_{55}^{**} = -Q_{22}^{*xyz(2)}$$

$$a_{56} = e_{31} A_{xy}^{z(1)} \frac{1}{R_y} - e_{31} A_{x}^{z(0)} \quad , \quad a_{57} = f_{31} A_{xy}^{z(1)} \frac{1}{R_y} - f_{31} A_{x}^{z(0)} \quad , \quad a_{66} = -h_{33} (\frac{\pi}{h})^2 A_{xmy}^{*z(0)}$$

$$a_{67} = -g_{33} (\frac{\pi}{h})^2 A_{xmy}^{*z(0)} \quad , \quad a_{77} = -\mu_{33} (\frac{\pi}{h})^2 A_{xmy}^{*z(0)}$$

Appendix D: The stiffness and mass matrices

The stiffness and mass matrices are described as follows:

$$K_{11} = a_{11} - a_{11}^{*} \alpha_m^2 - a_{11}^{**} \beta_n^2 \qquad K_{12} = -a_{12} \alpha_m \beta_n \qquad K_{13} = a_{13} \alpha_m - a_{13}^{*} \alpha_m^3 - a_{13}^{**} \alpha_m \beta_n^2$$
$$K_{14} = a_{14} - a_{14}^{*} \alpha_m^2 - a_{14}^{**} \beta_n^2 \qquad K_{15} = -a_{15} \alpha_m \beta_n \qquad K_{22} = a_{22} - a_{22}^{*} \alpha_m^2 - a_{22}^{**} \beta_n^2 \tag{D-1}$$
$$K_{23} = a_{23} \beta_n - a_{23}^{*} \beta_n^3 - a_{23}^{**} \alpha_m^2 \beta_n \qquad K_{24} = -a_{24} \alpha_m \beta_n \qquad K_{16} = a_{16} \alpha_m \qquad K_{17} = a_{17} \alpha_m$$

$$K_{25}=a_{25}-a_{25}^{*}\alpha_m^2-a_{25}^{**}\beta_n^2 \qquad K_{33}=a_{33}-a_{33}^{*}\alpha_m^2-a_{33}^{**}\beta_n^2+a_{33}^{***}\alpha_m^2\beta_n^2+a_{33}^{2*}\alpha_m^4+a_{33}^{2**}\beta_n^4$$

$$K_{34}=-a_{34}\alpha_m+a_{34}^{*}\alpha_m^3+a_{34}^{**}\alpha_m\beta_n^2 \qquad K_{35}=-a_{35}\beta_n+a_{35}^{*}\beta_n^3+a_{35}^{**}\alpha_m^2\beta_n$$

$$K_{36}=a_{36}\ ,\ K_{37}=a_{37}\quad K_{26}=a_{26}\beta_n\ ,\ K_{27}=a_{27}\beta_n \qquad K_{44}=a_{44}-a_{44}^{*}\alpha_m^2-a_{44}^{**}\beta_n^2$$

$$K_{45}=-a_{45}\alpha_m\beta_n \qquad K_{46}=a_{46}\alpha_m\ ,\ K_{47}=a_{47}\alpha_m\ K_{55}=a_{55}-a_{55}^{*}\alpha_m^2-a_{55}^{**}\beta_n^2$$

$$K_{56}=a_{56}\beta_n\ ,\ K_{57}=a_{57}\beta_n\quad K_{66}=a_{66}\ K_{67}=a_{67}\quad K_{77}=a_{77}$$

$$M_{11}=I_{11}^{*}+2I_1^{*3}c_1^{*}\frac{(\alpha_1-1)}{R_x}+I^{*6}c_1^{*2}\frac{(\alpha_1-1)^2}{R_x^2}$$

$$M_{12}=0\ ,\quad M_{13}=I_1^{*3}c_1^{*}\alpha_m+I^{*6}c_1^{*2}\frac{(\alpha_1-1)}{R_x}\alpha_m$$

$$M_{14}=I_1^{*1}+I^{*4}c_1^{*}\frac{(\alpha_1-1)}{R_x}+I_1^{*3}c_1^{*}+I^{*6}c_1^{*2}\frac{(\alpha_1-1)}{R_x}$$

$$M_{15}=0\ ,\quad M_{16}=0\ ,\quad M_{17}=0$$

$$M_{22}=I_{22}^{*}+2I_2^{*3}c_2^{*}\frac{(\alpha_2-1)}{R_y}+I^{*6}c_2^{*2}\frac{(\alpha_2-1)^2}{R_y^2} \tag{D-2}$$

$$M_{23}=I_2^{*3}c_2^{*}\beta_n+I^{*6}c_2^{*2}\frac{(\alpha_2-1)}{R_y}\beta_n$$

$$M_{24}=0\ ,\quad M_{26}=0\ ,\quad M_{27}=0$$

$$M_{25}=I_2^{*1}+I^{*4}c_2^{*}\frac{(\alpha_2-1)}{R_y}+I_2^{*3}c_2^{*}+I^{*6}c_2^{*2}\frac{(\alpha_2-1)}{R_y}$$

$$M_{33}=I^{*6}c_1^{*2}\alpha_m^2+I^{*6}c_2^{*2}\beta_n^2+\mathrm{I}^{*0} \qquad M_{34}=I^{*4}c_1^{*}\alpha_m+I^{*6}c_1^{*2}\alpha_m$$

$$M_{35}=I^{*4}c_2^{*}\beta_n+I^{*6}c_2^{*2}\beta_n\ ,\ M_{36}=0\ ,\ M_{37}=0 \qquad M_{44}=I^{*2}+2I^{*4}c_1^{*}+I^{*6}c_1^{*2}$$

$$M_{45}=0\ ,\quad M_{46}=0\ ,\quad M_{47}=0 \qquad M_{55}=I^{*2}+2I^{*4}c_2^{*}+I^{*6}c_2^{*2}$$

$$M_{56}=0\ ,\quad M_{57}=0\ ,\quad M_{66}=0 \qquad M_{67}=0\ ,\quad M_{77}=0$$

Nomenclature

NSGT	non-local strain gradient theory	FSDT	higher-order shear deformation theory
GPLs	graphene platelets	GPLRC	GPL reinforced composite
GPL-A	asymmetric distribution of GPL	GPL-S	symmetric distribution of GPL
GPL-U	unioform distribution of GPL	type 1	symmetric porosity
type 2	asymmetric porosity	type 3	uniform porosity
ρ_c	the density of porous core	V_{GPL} , V^m	the volume fraction of GPL and matrix
L_x , L_y	length	ρ_{GPL} , ρ^m	the density of GPL and matrix
h	total thickness	u_i $i = x, y, z$	the components of displacements at a distance z from the mid-plane $z = 0$
h_c	the thickness of the porous core	u , v , w	the components of displacements in the mid-plane
h_b	the thickness of bottom face sheet	ϕ_j $j = x , y$	the slope of double-curved sandwich panel
h_t	the thickness of top face sheet	ε_{ij} $i , j = x , y , z$	the components of normal and shear strains
x , y , z	the coordinate axes	σ_i $i = x, y, z$	the normal stress along off-axis coordinates
ϕ	panel angle	ε_i $i = x, y, z$	the normal strains along off-axis coordinates
a , b	the arc length of the panel	τ_{ij} $i, j = x, y, z$	the shear stresses
υ_{ij} $i, j = x, y, z$	the Poisson's ratio along off-axis coordinates	γ_{ij} $i, j = x, y, z$	the shear strains
$E_i , i = x, y, z$	elastic modulus for off-axis	E_i , $i = t, c, b$	elastic modulus for porous core and face sheets
η_i $i = 1,2,3$	the CNT efficiency parameters	Q_{ij} $i , j = 1$ *to* 6	the coefficients of the stiffness matrix
δU	the variations of the potential energy	δT	the variations of the kinetic energy
δV	the variations of the work of the external force	υ_{GPL} , υ^m	the Poisson's ratio of GPL and matrix
l_m	the small-scale parameter	$e_0 a$	Eringen's non-local parameter
I^{*i}	the mass moments of inertia	∇^2	Laplacian operator
C_{ijkl}	fourth-order stiffness tensor along the off-axis coordinates coordinates	σ_{ij} and ε_{kl}	the components of stress and strain along the off-axis
ϖ	the dimensionless natural frequency	e_{ikl}	piezoelectric
q_{ikl}	magnetic	s_{ik}	dielectric permeability
d_{ik}	electromagnetic coupling	μ_{ik}	magnetic permeability
ϕ	electric potential	Ψ	magnetic potential
E	electric field	H	magnetic field
V_0	inertial electric voltage	ψ_0	inertial magnetic potential